The research of SvS has been made possible by financial support from the Royal Netherlands Academy of Arts and Sciences (KNAW).

References

CATTI, M. & FERRARIS, G. (1976). *Acta Cryst.* A**32**, 163-165.

CUMMINS, H. Z. (1990). *Phys. Rep.* **185**, 211-409.

HALL, S. R. & STEWART, J. M. (1990). Editors. *XTAL*3.0 *Users Manual.* Univs. of Western Australia, Australia and Maryland, USA.

JANNER, A. & JANSSEN, T. (1980). *Acta Cryst.* A**36**, 408-415.

JANNER, A., JANSSEN, T. & DE WOLFF, P. M. (1983). *Acta Cryst.* A**39**, 658-666.

KATO, K. (1990). *Acta Cryst.* B**46**, 39-44.

MAKOVICKY, E. & HYDE, B. G. (1981). *Struct. Bonding (Berlin)*, **46**, 101-170.

MERMIN, N. D. & LIFSHITZ, R. (1992). Preprint.

ONODA, M., KATO, K., GOTOH, Y. & OOSAWA, Y. (1990). *Acta Cryst.* B**46**, 487-492.

PETŘÍČEK, V. (1989). *Acta Cryst.* A**45**, 61-63.

PETŘÍČEK, V., MALY, K. & CISAROVA, I. (1991). In *Methods of Structural Analysis of Modulated Structures and Quasicrystals*, edited by J. M. PÉREZ-MATO, F. J. ZUNIGA, G. MADARIAGA & A. LOPEZ-ECHARRI, pp. 262-267. Singapore: World Scientific.

PETŘÍČEK, V., MALY, K., COPPENS, P., BU, X., CISAROVA, I. & FROST-JENSEN, A. (1991). *Acta Cryst.* A**47**, 210-216.

SHELDRICK, G. M. (1976). *SHELX*76. Program for crystal structure determination. Univ. of Cambridge, England.

SMAALEN, S. VAN (1989). *J. Phys. Condens. Matter*, **1**, 2791-2800.

SMAALEN, S. VAN (1991*a*). *Phys. Rev. B*, **43**, 11330-11341.

SMAALEN, S. VAN (1991*b*). In *Methods of Structural Analysis of Modulated Structures and Quasicrystals*, edited by J. M. PÉREZ-MATO, F. J. ZUNIGA, G. MADARIAGA & A. LOPEZ-ECHARRI, pp. 90-106. Singapore: World Scientific.

SMAALEN, S. VAN (1991*c*). *J. Phys. Condens. Matter*, **3**, 1247-1263.

SMAALEN, S. VAN (1992). *Incommensurate Sandwiched Layered Compounds*, edited by A. MEERSCHAUT. Aedermansdorf: Trans Tech Publications. In the press.

SMAALEN, S. VAN, MEETSMA, A., WIEGERS, G. A. & DE BOER, J. L. (1991). *Acta Cryst.* B**47**, 314-325.

STEURER, W. (1990). *Z. Kristallogr.* **190**, 179-234.

WIEGERS, G. A., MEETSMA, A., HAANGE, R. J. & DE BOER, J. L. (1992). *J. Alloys Compds*, **178**, 369-378.

WIEGERS, G. A., MEETSMA, A., VAN SMAALEN, S., HAANGE, R. J., WULFF, J., ZEINSTRA, T., DE BOER, J. L., KUYPERS, S., VAN TENDELOO, G., VAN LANDUYT, J., AMELINCKX, S., MEERSCHAUT, A., RABU, P. & ROUXEL, J. (1989). *Solid State Commun.* **70**, 409-413.

WOLFF, P. M. DE, JANSSEN, T. & JANNER, A. (1981). *Acta Cryst.* A**37**, 625-636.

YAMAMOTO, A. (1985). *REMOS*85.0. Program for refinement of modulated structures. National Institute for Research of Inorganic Materials, Sakura-mura, Niihari-gun, Ibaraki 305, Japan.

ZUCKER, U. H., PERENTHALER, E., KUHS, W. F., BACHMANN, R. & SCHULZ, H. (1983). *J. Appl. Cryst.* **16**, 358.

Acta Cryst. (1992). A**48**, 618-625

The Incommensurate Structure of $(Sr, Ca)_{14}Cu_{24}O_{41}$: a Study by Electron Diffraction and High-Resolution Microscopy

BY O. MILAT,* G. VAN TENDELOO AND S. AMELINCKX

University of Antwerp (RUCA), Groenenborgerlaan 171, *B*2020 *Antwerp, Belgium*

AND M. MEHBOD AND R. DELTOUR

Université Libre de Bruxelles, CP 233, *bd de Triomphe, B*1050 *Brussels, Belgium*

(*Received* 15 *November* 1991; *accepted* 17 *February* 1992)

Abstract

The modulated structure in $(Sr, Ca)_{14}Cu_{24}O_{41}$ has been studied using electron diffraction and high-resolution microscopy. The structure can be considered as consisting of two interpenetrating substructures. The first sheet-like substructure is shown to be hardly modulated while the second substructure, consiting of c-oriented chains, contains most of the modulation. High-resolution electron microscopy allows either separate imaging of the two substructures or identification of the misfit between them.

* Permanent address: University of Zagreb, Institute of Physics, Bijenicka 46, 41000 Zagreb, Croatia.

0108-7673/92/040618-08$06.00

© 1992 International Union of Crystallography

1. Introduction

The compound $(Sr, Ca)_{14}Cu_{24}O_{41}$ was discovered by Subramanian, Torardi, Calabrese, Gopalakrishnan, Morrisey, Askew, Flippen, Chowdhry & Sleight (1988) as an unwanted by-product of the crystal growth of Bi-based superconducting materials, and by Mehbod, Van Lathem, Deltour, Duvigneaud, Wyder, Verwerft, Van Tendeloo & Van Landuyt (1990) as the secondary phase in iron-doped Bi-Sr-Ca-Cu-O superconducting compounds. Although the present material is semiconducting and not superconducting, it is of interest because of its peculiar structure, which was determined by X-ray diffraction soon after the discovery of this new phase (McCarron,

Subramanian, Calabrese & Harlow 1988; Siegrist, Schneemeyer, Shunsine, Waszcak & Roth, 1988). These studies have shown the structure to be incommensurately modulated, and could be treated as suggested by de Wolff, Janssen & Janner (1981).

Electron diffraction patterns described by Wu & Horiuchi (1991) exhibit diffuse streaks that have been attributed to 'initial phase disorder' of modulated chains on one sublattice of the structure; the second sublattice also being modulated but phase ordered. After this paper was submitted, real-space information (from high-resolution electron microscopy) on this particular modulation also became available (Wu, Takayamo-Muromachi, Suehara & Horiuchi, 1991). In that paper, the authors made use of conventional high-resolution electron microscopy. It is the purpose of this paper to describe studies using selective imaging techniques and to present a model for the incommensurate modulation.

The structure determined by X-ray diffraction is the average structure; high-resolution electron microscope studies can provide complementary information on local structures. This is particularly relevant for modulated phases where such local structures are, as a rule, different from the average structure. Moreover, since in the present case the two substructures have rather well separated diffraction patterns, it is in principle possible to image the two structures separately along selected directions.

2. Structural considerations

The crystal structure as derived by McCarron, Subramanian, Calabrese & Harlow (1988) consists of two interpenetrating structures based on two different sublattices. One sublattice (I) is face-centred orthorhombic with lattice parameters $a = 11.4$, $b = 12.9$, $c_I = 3.91$ Å. The structure based on this sublattice consists of sheets parallel to the *ac* plane formed by zigzag chains of edge-sharing square-planar CuO_4 clusters, of the same type as the double chains that occur in $YBa_2Cu_4O_8$ (Marsh, Flaming, Mandich, De Santolo, Kuo, Hong & Martinez-Miranda, 1988) and $SrCuO_2$ (Teske & Müller-Buschbaum, 1970). These chains are interconnected by bridging O atoms. This essentially planar arrangement is represented in Fig. 1(*a*). On both sides of this sheet the Ca/Sr ions occupy sites that are positioned along **b** in the centres of the large squares in this arrangement, indicated by crosses in Fig. 1(*a*).

The second sublattice (II) is also face-centred orthorhombic with the same lattice parameters *a* and *b* as sublattice (I), but with a different *c* parameter: $c_{II} = 2.75$ Å. The structure consists of planar chains parallel to the *c* direction, of edge-sharing square CuO_4 clusters, arranged as shown in Fig. 1(*b*) when projected on the *ac* plane. Successive chains along the *a* direction form a staggered arrangement in this plane. Since sublattice (II) is face-centred, the arrangement of chains along the *b* direction is also staggered.

The succession of atomic layers along the *b* direction can thus be represented as ...–[(Sr, Ca)–Cu_2O_3–(Sr, Ca)]–[CuO_2]–... where the layers between brackets refer to sublattices (I) and (II) respectively. The planar CuO_2 chains along **b** fit between the layers of Sr/Ca ions (Fig. 1*c*), leading to a variable coordination of the Sr/Ca ions.

3. Experimental

$(Sr, Ca)_{14}Cu_{24}O_{41}$ needle-shaped crystals have been obtained as a by-product of the growth of pure and doped Br–Sr–Ca–Cu–O single crystals. An alumina crucible of high purity has been used to avoid contamination. As a flux composition we have chosen Bi–Sr_2–Ca_2–Cu_2 using Bi_2O_3, $SrCO_3$, $CaCO_3$ and CuO as raw materials. The starting materials were ground, heated in air at 1193 K for 5 h, then cooled to 913 K at a rate of 0.5 K h^{-1} and followed by cooling to room temperature in the furnace. Single crystals were isolated mechanically.

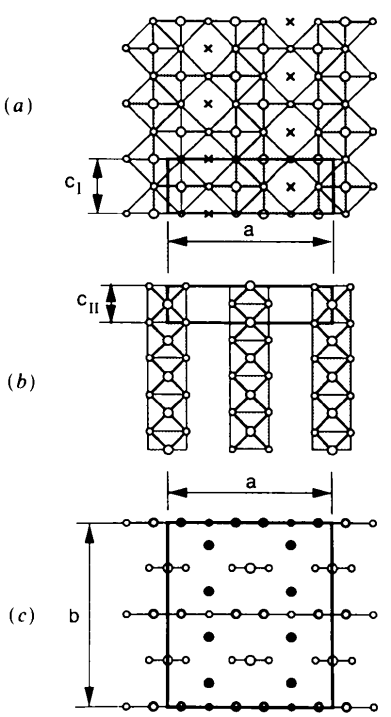

Fig. 1. Structural model of the compound $(Sr, Ca)_{14}Cu_{24}O_{41}$. (*a*) Structure of the Cu_2O_3 zigzag chains in the 'sheet' layer viewed along [010]. (*b*) Structure of the CuO_2 'chain' layer viewed along [010]. (*c*) Spatial arrangement of the constituent layers viewed along [001]. Cu–O bonds are indicated by full lines; CuO_4 squares are lightly shaded. The large open circles represent Cu, the small open ones O and the large filled ones Sr or Ca ions. The crosses in (*a*) indicate the positions of the Sr and/or Ca ions above and below the 'sheet'.

Samples for electron microscopy were prepared by simply crushing the needles and dispersing the powder on a copper grid dipped in a soft glue. The material was studied in a Philips CM 20 analytical electron microscope allowing the exploration of reciprocal space and in a JEOL 4000EX for the high-resolution observations. High-resolution images were obtained in the usual bright-field as well as in the dark-field mode; the modulation aspects have been studied using the latter.

4. Results

4.1. *Electron diffraction patterns*

From a number of electron diffraction patterns (EDP) it is clear that the reciprocal space can be regarded as consisting of two sublattices with somewhat different unit cells. Sublattice (I) is formed by the intense circular spots. From its c parameter [$c_I^* = (3.91\ \text{Å})^{-1}$], one can conclude that it is the reciprocal lattice of the structure consisting of Cu_2O_3 sheets and of layers of Sr/Ca atoms. Only spots with unmixed indices are present. Sublattice (II) is the reciprocal lattice of the structure formed by the CuO_2 chains, since the c parameter is $c_{II}^* = (2.75\ \text{Å})^{-1}$. It consists of spots that are streaked to some degree in all directions except [001]. From tilting experiments it can be deduced that the streaks are due to the intersections of the Ewald sphere with planes of diffuse intensity (replanes) parallel to (001)*.

The EDP along [001], shown in Fig. 2(a) consists only of sharp spots and exhibits a single unit mesh $2a^* \times 2b^*$, which proves that the two sublattices have a common mesh in this reciprocal plane. The absence of streaks is consistent with the geometry of replanes mentioned above, since these are parallel with the present section.

The [100] zone pattern of Fig. 2(b) shows that the b^*c^* plane consists of two types of reflections that belong to the two sublattices; the unit meshes of the two sublattices are indicated. Again, only spots with unmixed indices are present. Note the quasi-continuous streaks perpendicular to $\mathbf{c}^*$ with reinforcements at the spot positions of sublattice (II). The rows of weak spots closer to [010]* than the rows of strong spots are generated by double diffraction between the two sublattices; they are streaked because one of the two sublattices produces diffuse spots.

The [110] zone pattern of Fig. 2(c) also reveals the presence of additional spots between the nodes of the two sublattices. The unit mesh of this pattern is a centred rectangle for both sublattices, which is consistent with a body-centred reciprocal lattice, *i.e.* with a face-centred direct lattice for both structures.

The reciprocal lattice as projected along the a^* direction is shown in Fig. 3 [the corresponding EDP is shown in Fig. 2(b)]. From this projection it is clear

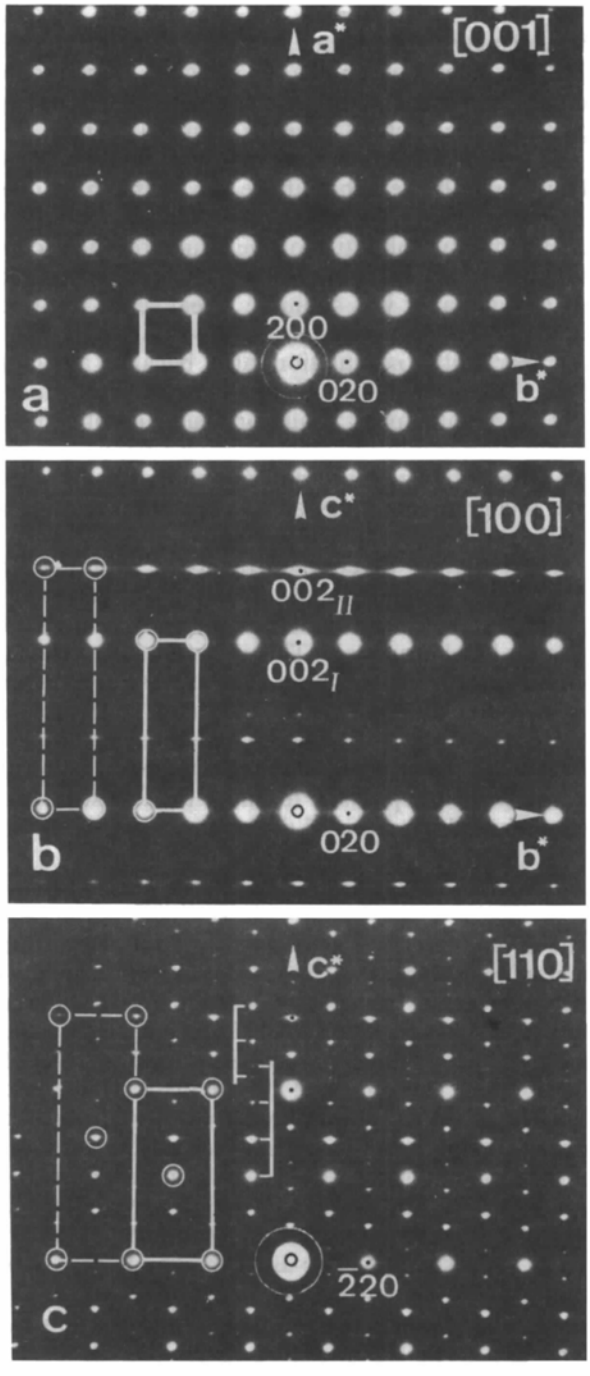

Fig. 2. Electron diffraction patterns of $(Sr, Ca)_{14}Cu_{24}O_{41}$. ($a$) The [001] direction. Only sharp spots with unmixed indices are present, defining a unique rectangular mesh. (b) The [100] direction. Two types of spots are present: (I) sharp circular; (II) weak, streaked. The unit meshes of the two sublattices are indicated – the (a^*, c_I^*) cell by full lines and the (a^*, c_{II}^*) cell by dashed lines. (c) the [110] direction. This section of reciprocal space also contains sharp circular reflections that can be regarded as basic ones and streaked spots, which can be considered as their satellites along the [001]* direction. Centred unit meshes for the two types of spots and the satellite sequences belonging to two neighbouring basic spots are indicated; note the spacing anomaly.

that the two sublattices can be revealed selectively by choosing respectively a section $(011)_{\mathrm{I}}^*$ for sublattice (I) and a section $(011)_{\mathrm{II}}^*$ for sublattice (II). The two sections differ by an angle of about 5° when rotated around the a^* axis. The first section is shown in Fig. 4(a); it exhibits sharp circular spots and only very weak residual streaks. This shows that the diffuse intensity is not spread uniformly over the (001)* replanes but concentrated in finite discs in the (001)* planes centred on the nodes of sublattice (II). On the other hand, the section $(011)_{\mathrm{II}}^*$ shown in Fig. 4(b) for sublattice (II) shows heavily streaked spots with only very weak sharp spots.

In the (010)* section of Fig. 4(c), as well as in the sections (100)* and (110)* - Figs. 2(b) and (c) respectively - the two sublattices are simultaneously revealed. They exhibit circular and streaked spots, but many more than would be present after a mere superposition of the two sublattices. In all sections where the two sublattices are excited simultaneously each spot of sublattice (I) is found to be the origin of a configuration of weaker spots with the geometry of sublattice (II) and *vice versa*. Except for the spots originating exclusively from sublattice (I), all other spots are streaked to some extent in a direction perpendicular to $\mathbf{c}^*$.

Alternatively, one can consider the strong circular spots as primary spots that can be attributed to a basic structure and the weaker and generally streaked spots as satellites associated with these basic spots. These satellite sequences are indicated by brackets in Fig. 2(c); their intensity decreases monotonically with increasing distance from the basic spot to which they belong. In Fig. 2(c) two or three satellites are visible on each side of the basic spots along the c^* direction. The separation of the satellites is given by: $\Delta g^* = c_{\mathrm{II}}^* - c_{\mathrm{I}}^*$. The real-space period corresponding to Δg^* is $1/\Delta g^* = 9.25$ Å. Where two satellite sequences belonging to different basic spots meet, a spacing anomaly, visible in Fig. 2(c), results.

All spots can be indexed rationally, to a first approximation, on a reciprocal lattice with base vectors a^*, b^*, $\frac{1}{3}\Delta g^*$. This was in fact the unit cell chosen for the X-ray structure determination by McCarron, Subramanian, Calabrese & Harlow (1988); in this way the structure was artificially made periodic and commensurate.

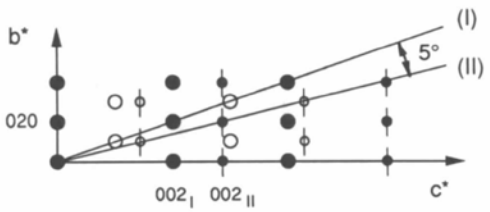

Fig. 3. Schematic representation of the reciprocal lattice as viewed along the a^* direction. Open symbols represent reciprocal-lattice nodes above (or below) the plane; two different dot sizes indicate two different sublattices. The (011)* sections of the sublattices I and II are indicated, as well as the tilting angle between them.

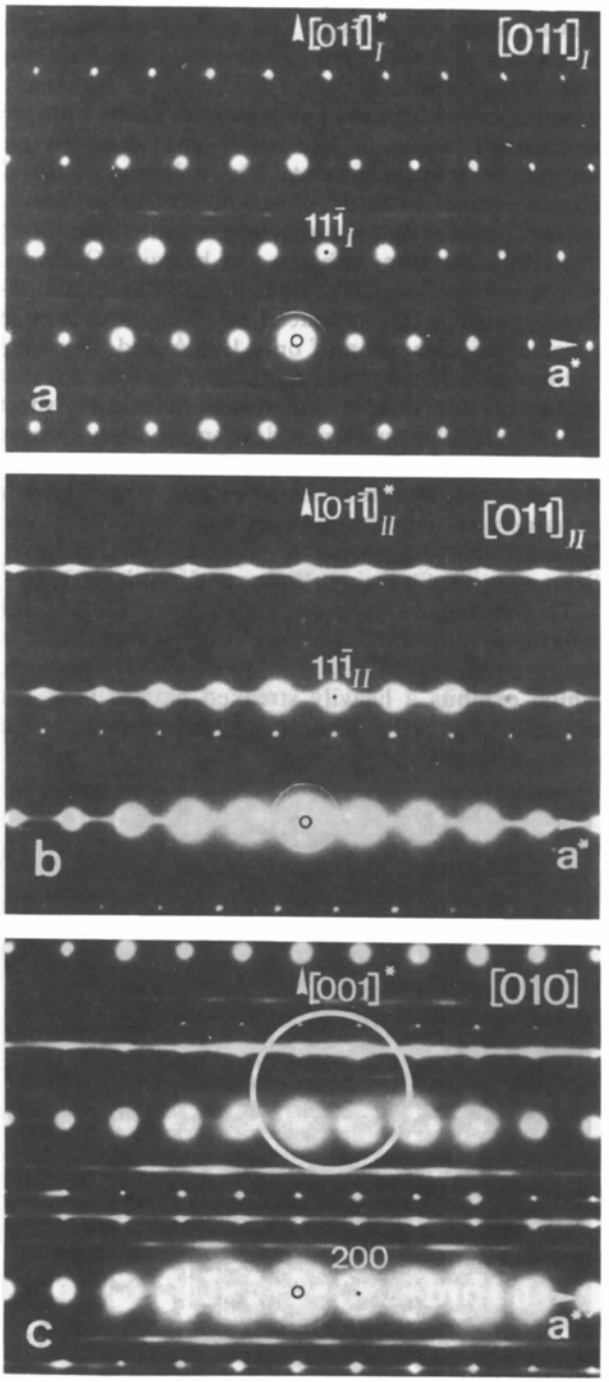

Fig. 4. Electron diffraction patterns of $(Sr, Ca)_{14}Cu_{24}O_{41}$, obtained by tilting around [100]. (a) The $(011)_{\mathrm{I}}^*$ section containing only the sharp spot pattern. (b) The $(011)_{\mathrm{II}}^*$ section containing only the streaked spot pattern. (c) The (010)* section. Note the presence of both the sharp and the streaked spots. The circle surrounds the reflections used to produce the dark-field image of Fig. 6.

4.2. *High-resolution images*

The simplest image, which moreover is not affected by disorder, is the one obtained along the *c* direction; it is reproduced in Fig. 5. The chains are in this case viewed along their length axis so longitudinal shifts of chains are not revealed. The unit mesh of the projected image has edges $a/2$ and $b/2$ in agreement with the centring of the structure; the actual unit cell is outlined in Fig. 5. The heavy-atom columns are imaged here as bright dots. The columns of Cu–O atoms parallel to the *c* direction project as closely spaced pairs within the sheets; they alternate along the [100] direction with rows of bridging O atoms, which are not revealed under the diffraction conditions used. The closely spaced Cu–O columns in each pair have a separation of only 1.96 Å and they were not resolved as separate bright dots; a single dot that represents the double column in the Cu_2O_3 sheet differs in brightness from a dot representing a single CuO_2 column in the chain layer. Fig. 5 clearly reveals the structural features present in Fig. 1(*c*), which is in agreement with the existing literature (McCarron, Subramanian, Calabrese & Harlow, 1988; Siegrist, Schneemeyer, Shunsine, Waszcak & Roth, 1988).

To visualize modulation defects more clearly, the intermediate-resolution image (Fig. 6) was made in the tilted dark-field mode along the [010] direction, which exhibits a heavily streaked pattern [see, for example, Fig. 4(*c*)]. The reflections selected for the image formation formed a rectangle consisting of four strong reflections: two sharp circular ones and two diffuse ones, as indicated in Fig. 4(*c*). The image can be considered as a mapping of the local Δg. The dot spacing along the rows perpendicular to **c** is now 4.6 Å $= \frac{1}{2} \times 9.2$ Å, which is the real-space separation corresponding to Δg^* in the satellite sequences, but taking into account the extinction of 001.

The vertical fringes in Fig. 6 with a spacing of 5.65 Å are produced by the interference between spots of the same sublattice, the main contribution coming from the intense sharp spots. They reveal the second harmonic of the *a* spacing. The intensity modulation with a period of 4.6 Å in most of these vertical bright fringes is due to the interference between a sharp and a diffuse spot. The spatial localization of the interference maxima in a given area is determined by the relative phase of the two beams that locally interfere in the area of foil considered. One of the interfering beams is produced by the 'sheet' sublattice (I) and the other one by the 'chain' sublattice (II); as a result, the localization of the modulation extrema (*e.g.* the bright dots) can provide information on the relative positions of the two sublattices. The 4.6 Å spacing is the second harmonic of the 9.2 Å spacing that was shown to be due to the periodic near coincidence of the two spacings c_I and c_{II}. Since both sublattices are face-centred, the 001 reflections are absent; therefore,

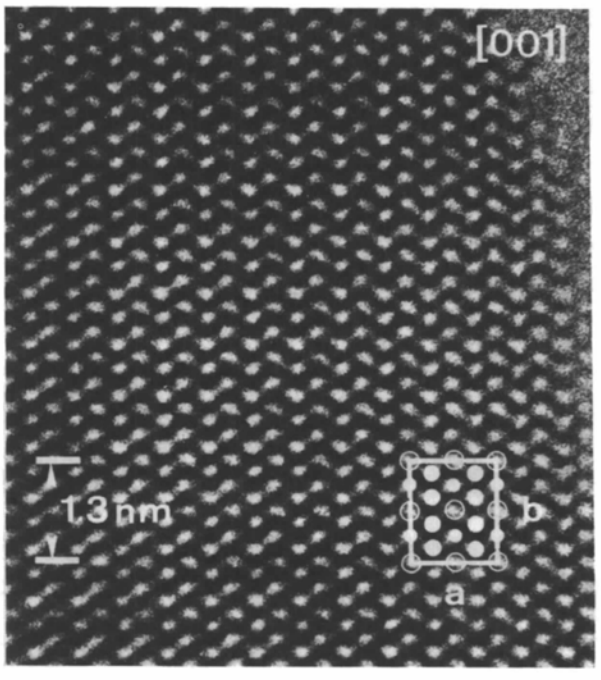

Fig. 5. High-resolution image of $(Sr, Ca)_{14}Cu_{24}O_{41}$ along [001]. The projected unit cell and the relation to the projected crystal structure of Fig. 1(*c*) are indicated. Open circles: Cu_2O_3 zigzag chains; larger dots: Sr/Ca atoms; smaller dots: CuO_2 chains.

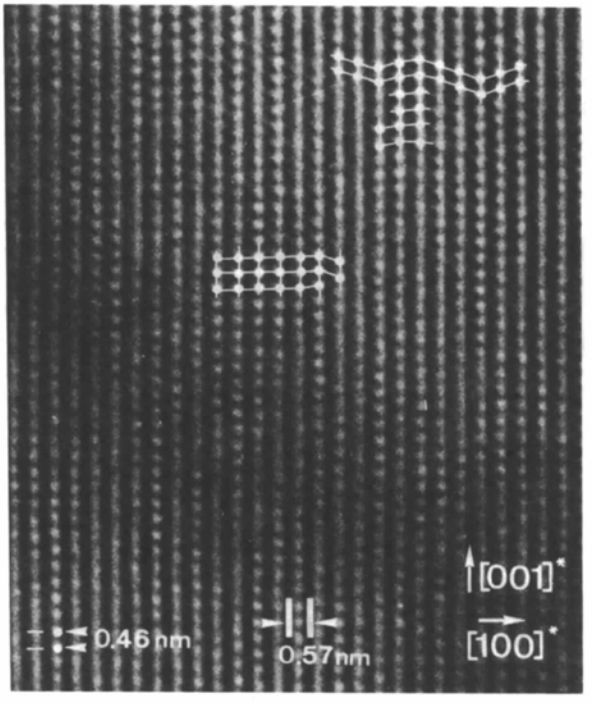

Fig. 6. Intermediate-resolution dark-field image of $(Sr, Ca)_{14}Cu_{24}O_{41}$ obtained by using the four strong spots of the (010)* section encircled in Fig. 4(*c*) to reveal local relative positions of the CuO_2 'chains' with respect to the Cu_2O_3 'sheets'.

only the second harmonic - 002 - can be used for imaging.

The rectangular geometry of the selected diffraction spots is normally expected to produce a rectangular pattern with unit mesh $a/2 \times \Delta g/2$. However, in certain areas, *e.g.* in Fig. 6, the rows of dots along successive vertical fringes are shifted and produce oblique parallelogram-shaped meshes. This clearly reveals that the relative positions of the double Cu_2O_3 chains in the sheets and of the single CuO_2 chains may be different in adjacent rows.

An alternative more structural way of reasoning relates the intensity extrema along the vertical bright fringes to quasi-coincidence columns resulting from the superposition of the Cu columns in the sheets and in the chains. The repeat period along c is 3.91 Å for the sheets, but the zigzag arrangement in the double chains along the c direction has a pseudo-period of half this spacing, *i.e.* of 1.96 Å. The quasi-coincidence period of $c_I/2$ and c_{II} is obviously 0.46 nm.

The bright-field high-resolution image along the [110] zone of Fig. 7 consists of sharp as well as diffuse spots, *i.e.* of spots belonging to both sublattices. In the thin parts the image reveals the crystal structure as projected along this zone. Again, the atom columns containing heavy atoms are revealed as bright dots (this is shown explicitly by Milat, Van Tendeloo & Amelinckx, 1992). It should be noted that along the rows of dots representing the (Sr, Ca) columns in Fig. 7 the brightness of the dots is somewhat variable, although the variation is not periodic. This can presumably be attributed to some variability in the Ca/Sr ratio along the columns.

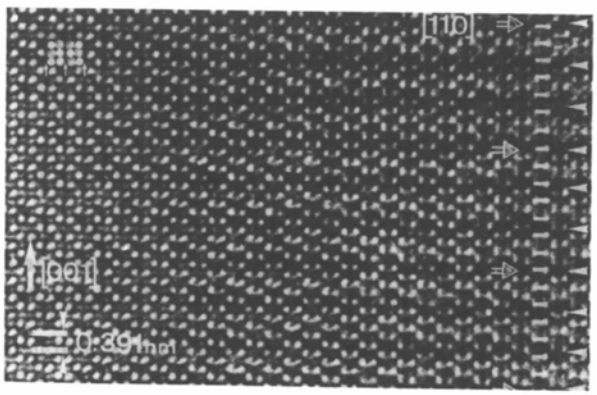

Fig. 7. High-resolution image of $(Sr, Ca)_{14}Cu_{24}O_{41}$ along [110]. The relation with the projected structure is indicated. Open circles: Cu atoms in Cu_2O_3 'sheets'; dots: Sr/Ca atoms; small arrows indicate lines where Cu atoms of CuO_2 'chains' project. The broad horizontal fringes with a 9.2 Å period in the thicker part of the wedge, indicated by arrows on the right side, reveal a brightness modulation along [001] which is incommensurate with respect to the basic substructure. Basic spacing of 3.91 Å = c_I and the near coincidence at $7c_I$ are indicated by a sequence of bars and open arrows, respectively.

In somewhat thicker parts of the wedge-shaped specimen, the dot pattern in Fig. 7 is brightness-modulated along **c**, giving rise to the broad fringes perpendicular to $\mathbf{c}^*$ with an average period of 9.2 Å (see the rows of double bright dots in Fig. 7). Closer examination of the brightness of these rows shows that the period is not quite constant, but that there is in fact a succession ... *LSS*... of two somewhat shorter spacings (S) alternating with a somewhat larger one (L). As a result, there is a 'superperiod' of 3×9.2 Å = 27.6 Å, which is close to the value of the c parameter of the coincidence unit cell adopted for the X-ray structure determinations. This c parameter is very nearly equal to the smallest common

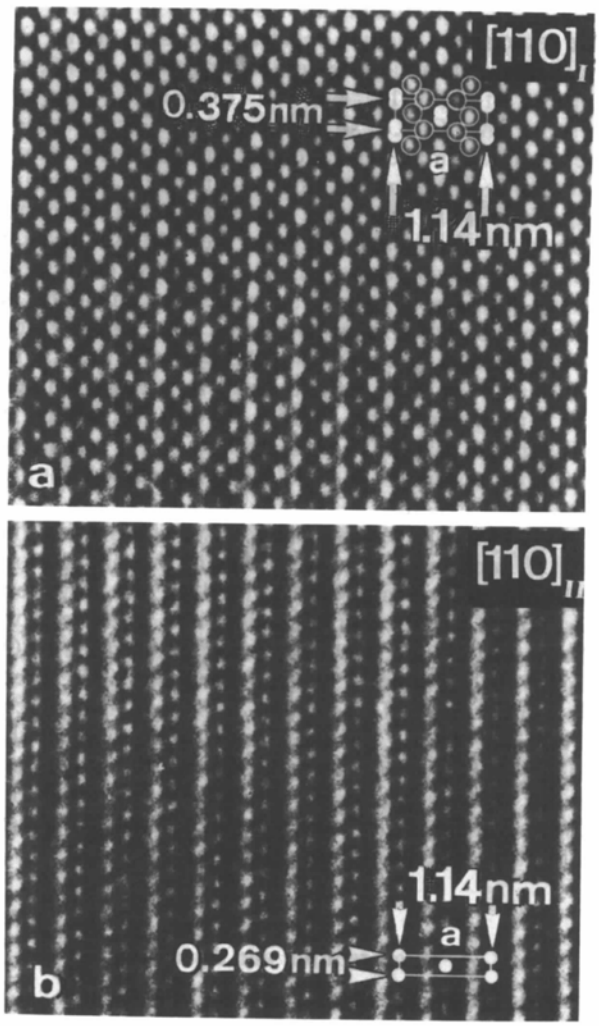

Fig. 8. High-resolution images of the two substructures separately in the same area of thin crystal of $(Sr, Ca)_{14}Cu_{24}O_{41}$. They reveal: ($a$) 'sheet' substructure by selecting spots belonging to the $(011)_I^*$ section only; a diffraction pattern along the same direction is shown in Fig. 4(a); (b) 'chain' substructure by selecting spots belonging to the $(011)_{II}^*$ section only; the corresponding diffraction pattern is shown in Fig. 4(b). Projected structures are indicated as in Figs. 5 and 7.

multiple of c_I and c_{II}, *i.e.* $7 \times c_I = 10 \times c_{II}$. The c_I period of 3.91 Å is prominently present in the direction of the rows of bright dots, *i.e.* along the c direction in Fig. 7. The broad fringes due to the brightness modulation are not always straight and perpendicular to the c direction. In some areas, especially when looking under grazing incidence at lower-magnification images, it becomes obvious that the broad fringes sometimes make a small angle with the normal to **c** and that they shift gradually sideways. This observation is relevant since it throws some light on the relative shifts of the 'sheet' and 'chain' substructures, as will be discussed below.

The images corresponding to the sections $(011)^*_I$ and $(011)^*_{II}$, reproduced in Figs. 8(*a*) and (*b*) respectively, are of particular interest since they reveal - in the same area - the two substructures separately. Fig. 8(*a*) shows the image corresponding to the sharp spot pattern of the $(011)^*_I$ section (see Fig. 4*a*); it represents the Cu_2O_3-'sheet' structure. The relation between the image and the projected structure along the same direction becomes clear when comparing Fig. 8(*a*) with Fig. 1(*a*); the CuO_2 chains do not appear in the image because they do not form a column-type configuration. All columns containing heavy atoms in the 'sheet' substructure can clearly be recognized as well separated bright dots. The brightest dots may be associated with the pair of Ca/Sr-atom columns, the less bright dots represent copper-containing columns (Milat, Van Tendeloo & Amelinckx, 1992). The periodicity of the projected structure along $[01\bar{1}]$ is 3.75 Å as expected for the 'sheet' substructure.

Fig. 8(*b*) shows the image associated with the $(011)^*_{II}$ section of Fig. 4(*b*). Again, the heavy-atom columns are revealed as bright dots, but now representing Cu in the CuO_2 'chains' (Fig. 1*b*). Therefore the period of 2.65 Å which corresponds to the CuO_2 chains, is dominantly present along the $[01\bar{1}]$ direction in the rows of less bright dots, *i.e.* between very bright but poorly resolved rows that represent the Cu_2O_3–Sr/Ca layers. Large areas of this image were found to reveal a periodic structure even though the diffraction spots are heavily streaked and the 'sheet' sublattice is certainly not columnar.

5. Interpretation and discussion

The observations will be interpreted in terms of two possible structural models.

The presence of diffuse insensity planes in reciprocal space is indicative of 'pencil disorder' in real space, *i.e.* the type of disorder occurring in an assembly of parallel linear strings of strictly equidistant scattering centres arranged in a two-dimensional lattice, but of which the longitudinal positions are disordered. The longitudinal relative shifts can be a non-negligible fraction of the repeat period along the strings. This type of disorder may result, for instance, if the linear strings are embedded in a matrix where open channels are available to accommodate the linear strings. Along such channels more than one stable or quasi-stable equilibrium position may exist. The diffuse planes in reciprocal space are then perpendicular to the strings and their separation is equal to the inverse of the repeat distance of the scattering centres along the linear strings.

A related type of disorder, which will produce similar diffraction effects, may occur in structures containing longitudinally modulated strings. In such structures the phases of the longitudinal modulation waves in neighbouring strings may be disordered, even though the equilibrium positions are essentially the same in all chains. In this case only small atomic displacements are sufficient to cause an appreciable change in the phase of the modulation wave. In this case diffuse planes pass through all modulation satellites; this has been shown explicitly by Wu & Horiuchi (1991). The latter situation is observed in the present case.

The selective imaging of the two sublattices can provide significant information on the relative magnitude of the displacements in the two sublatices. The image in Fig. 8(*a*), representing the 'sheet' structure, strongly suggests that this structure is either not at all or at most only weakly modulated. In any case it does not lead to displacements observable under high-resolution conditions. If one takes into account the heavy streaking of sublattice (II), the image of the 'chain' structure in Fig. 8(*b*) is still surprisingly well ordered, although with some visible deviations from strict periodicity. These deviations can best be observed under grazing incidence along the dense rows of dots. Comparing 'sheet' and 'chain' images we conclude that the 'sheet' sublattice is to a good approximation undeformed, the modulation being mainly confined to the 'chain' sublattice. Even in the latter case, the displacements involved are apparently rather small and do not lead to striking effects in a high-resolution image.

More striking evidence for the relative shifts of the two sublattices can be obtained from the dark-field image of Fig. 6, in which the structure is viewed along the b direction (*i.e.* along the normal to the layer planes). The bright dots along the rows parallel to the c axis vary in sharpness and in successive rows they are sometimes shifted relative to each other over observable distances, so as to generate parallelograms, instead of rectangles, which would be in agreement with the selected configuration of reflections in reciprocal space. This observation confirms, as explained above, that successive rows of 'chains' are in different relative positions with respect to the underlying 'sheet' structure. The better visibility of the shifts in this imaging mode is essentially due

to the 'vernier' effect described above, and which was exploited in this dark-field imaging mode.

Without having to specify which atom will occupy which 'hollow', it is possible to visualize how the 9.2 Å period results from the near coincidence of atomic positions. In Fig. 9 the 2.75 Å period has been schematically indicated by the upper row of bars; it can for instance be associated with the Cu atoms in the chains along the c direction in Fig. 1(b). In the lower row we have indicated by heavy bars the 3.91 Å period, and by dotted bars the 3.91/2 Å = 1.96 Å period. These periods can for instance be associated with the centres of the small squares [defined by the Cu-O bonds in Fig. 1(a)] in the sheet layer. Successive crystallographically equivalent sites are therein related by a 3.91 Å symmetry translation. However, the centres of the intermediate small squares could serve as possible almost equivalent sites. The Cu atoms of the chains would probably tend to occupy sites that project onto the centres of these small squares, but this is not essential for our reasoning. From consideration of the two parallel rows of bars, it becomes evident that near coincidence of heavy bars occurs at sites separated on average by 9.2 Å. In reality, the spacing between successive near-coincidence sites is not constant and consists, in Fig. 7, of two shorter segments alternating with one longer segment. In fact, the sequence will tend to be a 'uniform' mixture of spacings, approximating the average value. Similar observations of uniform mixtures of two periodicities are common knowledge in long-period-ordered alloys (Loiseau, Van Tendeloo, Portier & Ducastelle, 1985). If the equilibrium situation is assumed to correspond to the closest coincidence of the heavy bars, it is evident that small displacements in the sense indicated by arrows in Fig. 9 would tend to take place. This implies that certain segments are under tensile stress (indicated by '+'), while others would be under compressive stress (indicated by '−'). The overlap of '+' regions in one row with '−' regions in the neighbouring row corresponds to the situation of least strain energy, *i.e.* with a possible equilibrium situation.

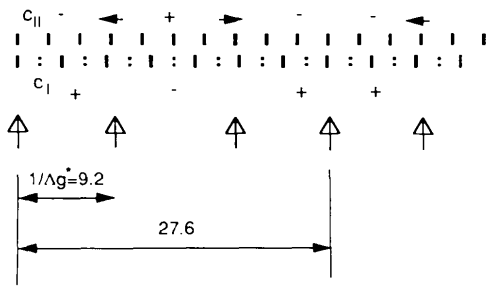

Fig. 9. Near-coincidence scheme of atomic positions in 'chain' (upper) and 'sheet' (lower) sublattices with their corresponding periodicities of $c_{II} = 2.75$ Å and $c_I = 3.91$ Å respectively. The average near-coincidence period $1/\Delta g^*$ deduced from electron diffraction is indicated by open arrows pointing up as well as the quasi-commensurate spacing 27.6 Å ($=3/\Delta g^* = 7c_I$). The accommodating strain and the regions of tensile and compressive stress are indicated by small arrows at the top, and by '+' and '−' signs, respectively. The upper signs refer to the upper layer, the lower signs to the lower layer.

The fact that the ratio of the sublattice parameters, c_I/c_{II}, is incommensurate and very close to $2^{1/2}$ favours the assumption that the building unit - square-planar CuO_4 - is very little distorted in the 'sheets' as well as in the 'chains'. This, however, is no proof, since the lattice parameters are average values only. Evidence for this assumption also comes from the lattice parameters of the isomorphous compounds in which different cations are substituted for (Ca, Sr) as in the work of Siegrist, Schneemeyer, Shunsine, Waszcak & Roth (1988). Such substitutions mainly affect the b parameter, as one would expect, since the size of these ions determines to a large extent the layer spacing. However, the effect on the c parameter is an order of magnitude smaller than that on the b parameter, which again is consistent with the assumption that the CuO_4 groups are rigid. On this basis it is to be expected that the incommensurateness will not be accommodated in localized discommensuration walls separated by commensurate domains but will at most lead to some mutual modulation of the two sublattices. The evidence suggests that the 'chain' lattice is likely to suffer the largest displacements, the 'sheet' lattice remaining rigid.

This work has been performed in the framework of the Belgian National Impulse Programme on High T_c Superconductivity under contract nos. SU/03/017 and SU/03/009, with the financial help of IUAP 11.

References

LOISEAU, A., VAN TENDELOO, G., PORTIER, R. & DUCASTELLE, F. (1985). *J. Phys. (Paris)*, **46**, 595-608.

MCCARRON, E. M. III, SUBRAMANIAN, A. M., CALABRESE, J. C. & HARLOW, R. L. (1988). *Mater. Res. Bull.* **23**, 1355-1365.

MARSH, P., FLAMING, R. M., MANDICH, M. L., DE SANTOLO, A. M., KUO, J., HONG, M. & MARTINEZ-MIRANDA, L. J. (1988). *Nature (London)*, **334**, 141-143.

MEHBOD, M., VAN LATHEM, E., DELTOUR, R., DUVIGNEAUD, P. H., WYDER, P., VERWERFT, M., VAN TENDELOO, G. & VAN LANDUYT, J. (1990). *Physica (Utrecht)*, **C168**, 265-271.

MILAT, O., VAN TENDELOO, G. & AMELINCKX, S. (1992). *Ultramicroscopy.* In the press.

SIEGRIST, T., SCHNEEMEYER, L. F., SHUNSINE, S. A., WASZCAK, J. V. & ROTH, R. S. (1988). *Mater. Res. Bull.* **23**, 1429-1438.

SUBRAMANIAN, M. A., TORARDI, C. C., CALABRESE, J. C., GOPALAKRISHNAN, J., MORRISEY, K. J., ASKEW, T. R., FLIPPEN, R. B., CHOWDHRY, U. & SLEIGHT, A. W. (1988). *Science*, **239**, 1015-1017.

TESKE, C. L. & MÜLLER-BUSCHBAUM, H. (1970). *Z. Anorg. Allg. Chem.* **379**, 134-143.

WOLFF, P. M. DE, JANSSEN, T. & JANNER, A. (1981). *Acta Cryst.* A**37**, 625-636.

WU, X. J. & HORIUCHI, S. (1991). *Acta Cryst.* A**47**, 11-26.

WU, X. J., TAKAYAMA-MUROMACHI, E., SUEHARA, S. & HORIUCHI, S. (1991). *Acta Cryst.* A**47**, 727-735.